Temporal Development of Backward Erosion Piping in a Large-Scale Experiment

Pol, J.C.; Kanning, W.; Jonkman, Sebastiaan N.

DOI
10.1061/(ASCE)GT.1943-5606.0002415

Publication date
2021

Document Version
Final published version

Published in
Journal of Geotechnical and Geoenvironmental Engineering

Citation (APA)
Pol, J. C., Kanning, W., & Jonkman, S. N. (2021). Temporal Development of Backward Erosion Piping in a Large-Scale Experiment. *Journal of Geotechnical and Geoenvironmental Engineering*, *147*(2), Article 04020168. https://doi.org/10.1061/(ASCE)GT.1943-5606.0002415

ASCE

Temporal Development of Backward Erosion Piping in a Large-Scale Experiment

Johannes C. Pol[1]; Willem Kanning, Ph.D.[2]; and Sebastiaan N. Jonkman, Ph.D.[3]

Abstract: This paper presents a large-scale backward erosion piping experiment aimed at studying the erosion rate. This temporal aspect of piping complements previous research that focused on the critical head. To study the progression rate in realistic conditions, an experiment was carried out on a 1.8 m high levee with a cohesive blanket on a sandy foundation. The pipe was guided along a row of pore pressure transducers in order to measure its temporal development. Pipe development in space and time was successfully derived from pore pressure changes, showing an average progression rate of 8 m/day during the progressive erosion phase. The results show a relation between upstream gradient and progression rate. Furthermore, analysis of the eroded sand mass shows a relatively large pipe volume compared to existing lab tests, and an approximately linear relation between pipe length and volume. The results and insights from this study can be used to validate and improve transient piping models, leading to more accurate dam and levee safety assessments. **DOI: 10.1061/(ASCE)GT.1943-5606.0002415.**

Introduction

Flooding is one of the most significant natural disasters worldwide (Jonkman 2005). The past decades have shown an increase in flood risk (Jongman et al. 2012; Paprotny et al. 2018), and without countermeasures, this is expected to further increase because of climatic and socioeconomic changes. A common strategy to reduce flood risk is using structural flood protection measures like levees and dams. Levee failure can occur because of a range of failure mechanisms such as overflow, slope instability, or internal erosion (Morris et al. 2008). This study focuses on the mechanism of backward-erosion piping (in short piping), which is a form of internal erosion. After overtopping, piping is considered one of the most hazardous failure mechanisms in dams (Foster et al. 2000) and river levees (Danka and Zhang 2015; Tóth and Nagy 2006; Jongejan and Maaskant 2015).

Piping Process

Piping occurs when seepage induced by a head difference (H) over the levee leads to erosion of a granular levee foundation, which is covered by a cohesive roof, to such extent that a hydraulic shortcut forms. The eroded grains settle around the outflow location as a sand boil. Fig. 1 shows a sketch of a typical levee sensitive to piping and the most important parameters. In areas with blankets (cohesive top layer on the land side) there are three necessary conditions to induce piping failure: (1) rupture of the land-side blanket, (2) transport of the granular material through the fault in the blanket, and (3) formation of a continuous pipe below the structure (Schweckendiek et al. 2014). This paper focuses on the third condition.

From the beginning of the twentieth century, extensive research has been done on the factors that determine the critical head difference (H_c) at which piping occurs (i.e., a fully developed erosion channel creating a full hydraulic shortcut resulting in a breach), for example Bligh (1910), Miesel (1978), Hanses (1985), Sellmeijer (1988), Schmertmann (2000), Van Beek (2015), Robbins et al. (2017), and Vandenboer (2019). The findings that are most relevant for this paper are discussed subsequently.

Based on a data set of dam and levee failures, Bligh (1910) observed that piping occurs if the global hydraulic gradient (head difference H divided by seepage length L) was larger than a critical creep value that depends on the type of soil.

Based on laboratory studies, Hanses (1985) noted that the erosion process includes both primary erosion (lengthening of the pipe) and secondary erosion (widening and deepening of the pipe). Both processes occur in conjunction: pipe lengthening results in higher flow rates and subsequent pipe deepening and widening. Miesel (1977) and Muller-Kirchenbauer (1980) observed that after initiation of erosion, the erosion often stopped and progressed only after a head increase. This equilibrium can be explained by several factors such as the convergence of flow to the exit.

An equilibrium curve (Fig. 2) shows pipe length (l) versus the head at which all grains are just in equilibrium (H_{eq}). The critical head (H_c), is the highest head at which equilibrium is possible. When the pipe grows longer than the corresponding critical length (l_c), equilibrium can only exist when the head is lowered sufficiently. A configuration is *progression dominated* if an equilibrium develops after an initial formation of a pipe, and is *initiation dominated* if this is not the case (Van Beek 2015) (Fig. 2). Levees with cohesive blankets are often progression dominated because of the concentrated outflow. The phases before and after the critical point are in this paper referred to as *regressive* and *progressive*, respectively (Fig. 2). Regressive means that an equilibrium is reached given a constant head, while progressive means that the pipe growth continues given a constant head.

[1]Researcher, Dept. of Hydraulic Engineering, Delft Univ. of Technology, Stevinweg 1, 2628 CN Delft, Netherlands; Flood Risk Consultant, Dept. of Rivers, Coasts and Deltas, HKV Consultants, Botter 11-29, Lelystad, Netherlands (corresponding author). ORCID: https://orcid.org/0000-0001-6895-8256. Email: J.C.Pol@tudelft.nl

[2]Researcher, Dept. of Hydraulic Engineering, Delft Univ. of Technology, Stevinweg 1, 2628 CN Delft, Netherlands; Flood Risk Advisor, Deltares, Boussinesqweg 1, 2628 CN Delft, Netherlands.

[3]Professor, Dept. of Hydraulic Engineering, Delft Univ. of Technology, Stevinweg 1, 2628 CN Delft, Netherlands.

Note. This manuscript was submitted on September 13, 2019; approved on July 27, 2020; published online on December 4, 2020. Discussion period open until May 4, 2021; separate discussions must be submitted for individual papers. This paper is part of the ***Journal of Geotechnical and Geoenvironmental Engineering***, © ASCE, ISSN 1090-0241.

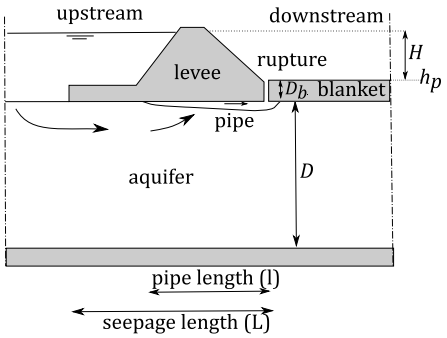

Fig. 1. Situation sketch of a typical piping problem for levees.

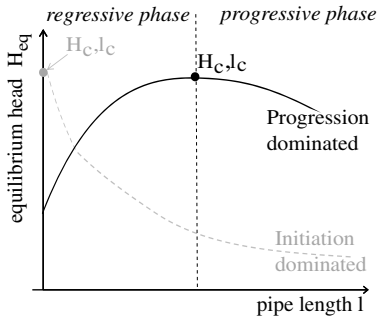

Fig. 2. Equilibrium curve. Regressive means that an equilibrium is reached given a constant head; progressive means that the pipe growth continues given a constant head.

In the Netherlands, levees are assessed and designed using the model of Sellmeijer (1988) or a simplified formula (Sellmeijer et al. 2011). Sellmeijer's model combines two-dimensional (2D) groundwater flow, pipe flow, and stability of grains on the pipe bed. As such, this stability criterion is based on secondary erosion. The model predicts an equilibrium curve similar to Fig. 2, which is also observed in experiments.

Time-Dependent Processes in Piping

Current steady piping models are focused on the critical head, but in some cases time-dependent processes can be relevant. Time dependence in the piping failure process includes three main components: (1) hydraulic load, (2) groundwater flow, and (3) pipe growth. The duration of the extreme hydraulic load (first component) is the driver: the shorter the load duration, the less time is available for the piping process to develop. A flood with limited duration, such as a storm surge, induces nonstationary seepage flow, which leads to delay and damping in the response of the aquifer pore pressure at the downstream side of the levee (second component). This reduces the potential for rupture of the blanket and initiation of piping, but also delays these events. This paper focuses on the third component: pipe growth. Once piping has initiated, it takes time to progress toward the upstream side and create a shortcut. If the load has reduced sufficiently in the meantime, the erosion process stops and failure is prevented. The pipe progression rate, v, either in the progressive or regressive phase, is defined as the increase in pipe length (l), over a given period of time (t).

Piping Experiments Including Temporal Development

A number of experiments include information about the development of the pipe over time. Experiments of the progression rate of piping at small and medium scale were recently carried out by Robbins et al. (2017), Vandenboer et al. (2019), and Allan (2018). Progression rates were also obtained by Pol et al. (2019) from a selection of small and medium scale tests by Van Beek (2015). Apart from scale effects, these laboratory experiments differ from field conditions in having a smooth, rigid roof above the sandy layer.

Two large scale piping experiments relevant to levees are: (1) Large scale tests in the Delta Flume at Deltares (W. de Rijke, Verificatie pipingmodel: Proeven in de deltagoot. Meetverslag., unpublished report), see also Rotunno et al. (2019). However, these tests were stopped just after the critical head was reached, so they include only a small part of the progressive phase. (2) Development of the pipe length in the IJkdijk large scale tests (Van Beek et al. 2010) is shown in Sellmeijer et al. (2011) and Parekh et al. (2016), based on pore pressure changes. The pipe pattern in these tests is 2D with multiple sand boils and pipes, caused by the plane type exit configuration. In combination with limited sampling, this creates substantial difficulties in determining the pipe length development. For instance, in Sellmeijer et al. (2011) the derived maximum pipe length in Test 1 and Test 3 is far less than the seepage length of 15 m. In Test 2, which is shown in both publications, a pipe length of 1.5 m is reached after almost 80 h according to Parekh et al. (2016) and after 50–65 h according to Sellmeijer et al. (2011).

Modeling Temporal Development of Piping

Several authors have modeled aspects of the temporal development of piping, such as an equilibrium condition in a transient groundwater flow model (Van Esch et al. 2013), secondary erosion rates in hole erosion tests (Bonelli and Benahmed 2010) and in laminar flow (Cheng 2004), and primary erosion rates (Kézdi 1979; Fujisawa et al. 2010; Wang et al. 2014; Rotunno et al. 2019). Although significant advancements were made in recent years, no model is known to the authors that includes both primary and secondary erosion mechanisms and that has been validated on a wide range of sands and test configurations. The model of Rotunno et al. (2019) contains both mechanisms and was applied to the IJkdijk and Delta Flume experiments, but requires calibration of the primary erosion coefficients.

Objective

Most piping research focuses on the critical head. Recent work also describes the temporal development in laboratory experiments, but there is still a need for a coherent predictive model of temporal development. To support the validation and development of such a model, this paper aims to study the temporal development of piping in terms of pipe progression rates during the progressive phase of a progression-dominated configuration. This is achieved by a large-scale experiment that reflects realistic conditions including a blanket and a hole-type exit, while monitoring the main parameters (pore water pressure, sand discharge, flow rate). The resulting data set is publicly available for other researchers to validate their models (Pol et al. 2020).

Experimental Setup

Dimensions of the Test Levee

The Flood Proof Holland test facility (Kreijns et al. 2018) was used to conduct the piping experiments on a large scale (i.e., representative of a real levee) but in a controlled environment. The design of the test levee was constrained by the test facility

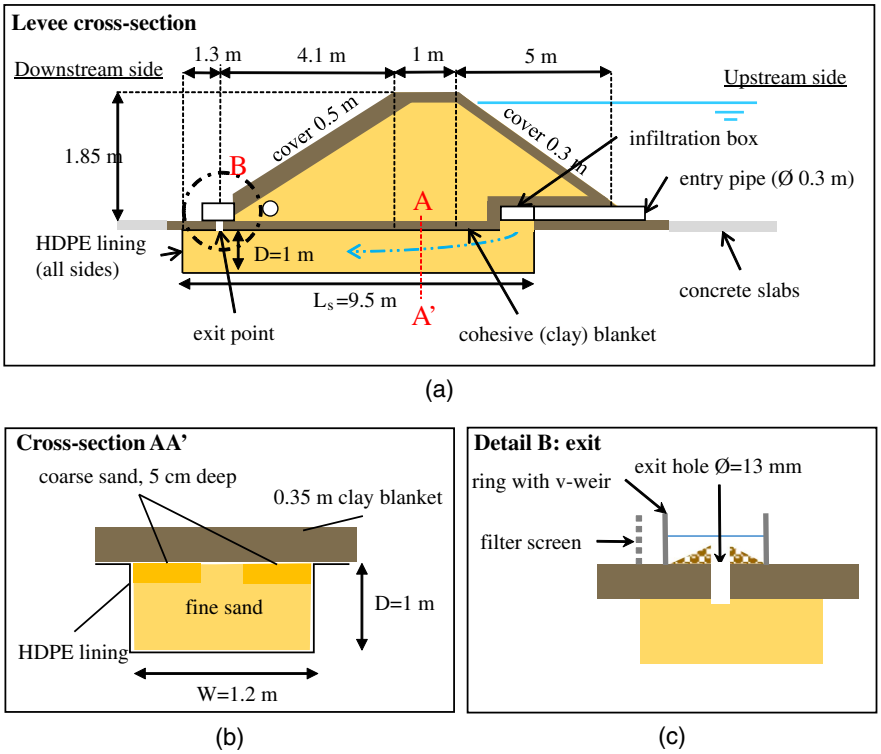

Fig. 3. Sketch of test levee design: (a) cross section of levee; (b) sand bed; and (c) detail of exit hole. Not to scale.

dimensions to a maximum levee height of 1.8 m, a minimum levee base length of 10 m, and a maximum aquifer depth of 1 m. Initial calculations with the model of Sellmeijer (2006) predicted no failure at the maximum head of 1.8 m and a seepage length of 10 m, regardless of sand type (fine or coarse). Therefore the seepage length was shortened by installing a pipe and infiltration boxes (Fig. 3). Undesired seepage to and from the sand bed was prevented by a HDPE geomembrane at the bottom and sides and a 0.35 m cohesive (clay) blanket that extends below the levee body, separating the levee body from the aquifer. This setup with blanket was chosen since this is the most common levee configuration in the Netherlands. The cohesive blanket allows for realistic sand/blanket interaction, as well as for deformation; both of which are not incorporated in laboratory experiments with a rigid transparent boundary.

The sand bed was rectangular with length $L_b = 9.5$ m, depth $D = 1$ m, and width $W = 1.2$ m. The seepage length, L, between the exit and downstream side of the infiltration box, was 7.2 m. The exit was a hole with a diameter of 13 mm. The fine sand (grain size $d_{50} = 185$ μm) was based on the lowest expected critical head. See Table 1 for details.

To measure water pressures in the pipe accurately, the pipe needs to grow under the pressure transducers. To prevent sideward pipe development, strips of coarse sand were included in the upper 0.05 m of the sand bed (Fig. 4). The shape of the strips minimizes disturbance of the process. First, the alternating pattern of coarse and fine sand prevents a strong preferential flow through the coarse sand. Second, the diagonal positioning prevents the pipes growing to the edges. Finally, the strips were relatively thin: 0.05 m compared to an aquifer thickness of 1.0 m. Uncertainties related to the coarse sand strips are discussed further in the "Discussion" section.

The sandy levee had a clay cover at the upstream side and crest as well as at the interface between sand bed and levee body. It had clayey, loamy, and sandy covers at the downstream side for overflow erosion tests [outside the scope of this paper; see Yagisawa et al. (2019)]. The tested cross section was at the interface of a loamy and sandy downstream slope. The entire levee was covered with grass sods. Because of the clay lining, the composition of the levee body has no significant influence on the piping process. See Fig. S1 for an overview of the levee and test basin.

Sand Properties

Table 1 shows the properties of the fine and coarse sands. For some parameters, multiple samples were tested, in which case the standard deviation, σ, and number of tests, N, are given. Some properties of the coarse sand were not relevant for the test and therefore not measured. Grain sizes ($d_{10} - d_{70}$) were obtained by sieving. The in situ porosity (n) was determined by pushing five thin-walled

Table 1. Properties of test materials

Parameter	Units	Fine sand μ (σ, N)	Coarse sand μ (σ, N)
d_{10}	μm	127 (3,3)	190 (—)
d_{50}	μm	185 (9,3)	400 (—)
d_{60}	μm	201 (3,3)	450 (—)
d_{70}	μm	223 (15,3)	500 (—)
ρ_s	kg/m^3	2,610 (5,2)	—
n	—	0.383 (0.005,4)	—
n_{min}	—	0.361 (—)	—
n_{max}	—	0.485 (—)	—
κ_{lab}	m^2	$1.2 \cdot 10^{-11}$ ($5.6 \cdot 10^{-12}$,6)	$4.1 \cdot 10^{-11}$ ($8.3 \cdot 10^{-13}$,3)
k_{lab} at 5°C	m/s	$8.0 \cdot 10^{-5}$ ($3.6 \cdot 10^{-5}$,6)	$2.6 \cdot 10^{-4}$ ($5.4 \cdot 10^{-6}$,3)
k_{levee}	m/s	$9 \cdot 10^{-5}$	—
C_u	—	1.59 (0.01,3)	2.4 (—)
D_r	—	0.823	—

J. Geotech. Geoenviron. Eng., 2021, 147(2): 04020168

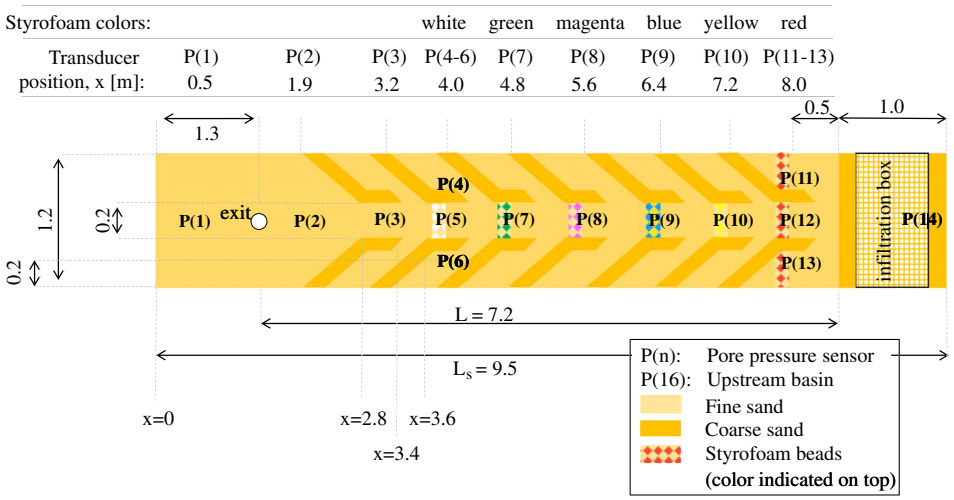

Fig. 4. Top view of sand bed showing exit, coarse sand strips, transducer position and styrofoam bead colors. Dimensions in meters. Not to scale.

steel cylinders horizontally into the upper layer of the sand bed, measuring their volume and weighing the oven-dried sand. Minimum and maximum porosity was estimated by compacting oven-dried sand in a cylinder. Particle density (ρ_s) was determined by a pyknometer (Duran, Mainz, Germany). Intrinsic permeability (κ_{lab}) was determined in the lab using a constant head test and converted to hydraulic conductivity for the field test temperature of 5°C (k_{lab}). The in situ hydraulic conductivity (k_{levee}) was determined using measured head, discharge, and Darcy's law. The coefficient of uniformity (C_u) and relative density (D_r) were calculated from the values given previously.

Monitoring Equipment

The main monitoring equipment consisted of 14 atmospheric pressure corrected pore-pressure transducers (First Sensor AG, Puchheim, Germany) placed on the interface of the sand bed and clay blanket, plus one in the upstream basin and one in the levee core. Fig. 4 shows their numbering. Their signal (1/10 Hz) was monitored in real time in the control room. Styrofoam beads (1–2 mm) with different colors were placed at the top of the sand bed at different distances along the expected pipe path (Fig. 4). The beads are used as a visual monitoring aid, where beads of a certain color appearing at the outflow point show that the pipe has at least passed the location associated with the bead color. Flow rate and sand discharge were measured at the exit hole location each 30–60 min, depending on the rate of erosion. A ø0.6 m bucket with cut-out bottom and a V-notch weir with an angle of $\theta = 55°$ was placed around the exit (Fig. S2). The flow rate, Q (m^3/s), was calculated from the water level, h_k (m), above the V-notch weir using (Shen 1981)

$$Q = 2.36 \cdot 0.577 \cdot \tan(\theta/2) \cdot (h_k + 0.00123)^{5/2} \qquad (1)$$

Eroded sand deposited around the exit hole was collected using a spoon. First, a small part (approximately 50 g) was stored for grain size analysis. The residual sand was supplemented with water up to a fixed volume (usually 400 mL) and the sand–water mixture was weighed. The dry sand mass (M) follows from the mass of the mixture and the water and sand densities. The mass of the small part and the residual were combined in a one time series. This in situ method was validated in the lab against oven-drying, which confirmed its suitability.

Construction Method

After excavation of a trench in the clay-peat subsoil, the HDPE geomembrane was placed in the trench and the fine sand was added and compacted in 0.20 m layers using a vibrating plate. After leveling the sand, the diagonal strips were carefully excavated using a trowel to a depth of 0.05 m, filled with coarse sand and compacted by tamping. The styrofoam beads were pushed in the sand bed and directly covered by clay. Then, the clay blanket was carefully placed on the sand by an excavator and compacted with a vibrating plate. Transducers were packed in a filter sleeve, installed in holes through the clay layer extending 10 mm into the sand bed, and sealed with bentonite. Finally, the levee was constructed on top of the blanket. There were four weeks between the installation of the transducers and the start of the experiment.

Test Procedure

At the start of the test, the pressures were constant and the pressure readings were set to a zero level. Then, the exit hole was created by piercing the cohesive blanket. The upstream basin level was initially raised in 0.3 m steps, which was reduced to 0.1 m steps at a basin level of 0.9 m. The level was only raised if no sand transport was observed for 30 min. Each 30–60 min, the exit location was inspected, discharge measured, and sand samples taken. The inspection interval was based on the rate of development of the process. The development of pore pressures was checked continuously for signs of erosion near one of the transducers, which is visible as pressure drop or peak in local gradient (Parekh et al. 2016; Robbins et al. 2017). The test was stopped by pumping the water out of the upstream basin when the pipe tip reached the upstream side of the sand bed ($x = 8$ m), which could be seen in the pressure measurements.

Results and Analysis

General Observations

The piping process went through the several phases described in literature (Van Beek 2015): seepage without sand transport, fluidization of sand in the exit hole, crater formation (Fig. S2), equilibrium (regressive phase), and ongoing erosion (progressive phase), see Fig. 5. It was observed visually that the sand deposition at the

J. Geotech. Geoenviron. Eng., 2021, 147(2): 04020168

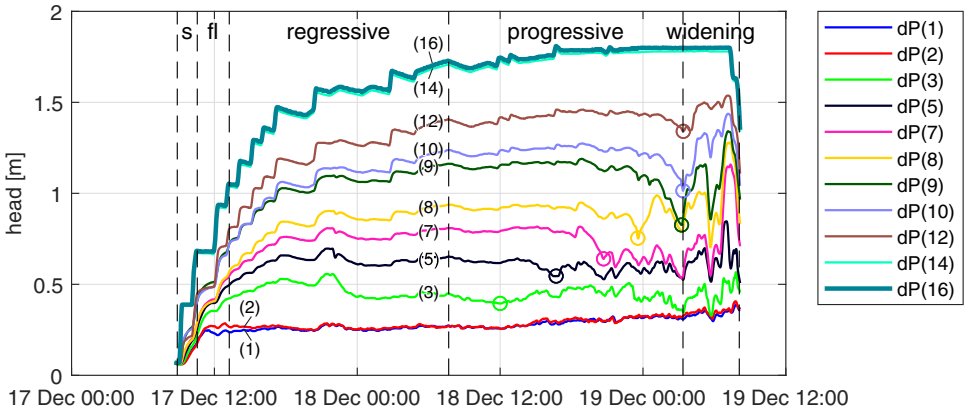

Fig. 5. Head at central row of transducers. Circles indicate assumed pressure stabilization point. P(16) is upstream basin level. s = seepage; and fl = fluidization.

exit is not continuous but intermittent. This may be caused by groups of grains being detached from the pipe tip, something that has been observed by many researchers, e.g., Van Beek et al. (2015) and Xiao et al. (2019).

The effects of piping erosion were clearly visible in the pore pressure measurements, which are the primary source of information in this experiment. Styrofoam beads from the pink, green and white strips were only observed at the end of the test, during the widening phase. Because the pipe must have passed the beads much earlier, it is suggested that the beads got stuck in the shallower parts of the pipe. However, it is unlikely that this influenced the flow or erosion process, since the pipe can easily grow around it. Because of the large delay, this method was not used to estimate pipe tip position. The method may only be successful in case of finer beads, with a diameter similar to the grain size. Furthermore, the discharge readings were not accurate enough to measure small changes. Therefore, only the order of magnitude is known, but is is not possible to detect significant changes during the test. These measurements should be more sensitive in future tests. The mass of the sand collected with a spoon shows a consistent trend . As the eroded sand cannot leave the bucket, the error in the cumulative mass will be small.

Head and Hydraulic Gradient

Pore Pressure Development

This section describes the measured pore pressures and hydraulic gradients, which form the basis for the analysis of progression rates. The following preprocessing steps were taken. The transducers were zeroed just before the test during no-flow conditions at an upstream level of 0.065 m, to ensure that all pressures are relative to the same reference level. Therefore, all measurements were increased by 0.065 m head. Furthermore, sensors P2 and P3 showed some sudden drops in pressure that could not be explained by physical behavior. These jumps of 2 kPa at the maximum were removed from the signal. It is noted that P2 and P3 do not affect the conclusions on the progression rates, as these transducers were passed when the flow was not yet in the progressive phase. Finally, the 0.1 Hz signal is smoothed using a 600 s moving average.

Fig. 5 shows the resulting head time series of each transducer in the central row. All heads are relative to the upstream basin floor. P16 is the upstream head, P1 is the most downstream transducer in the aquifer (Fig. 4). When the upstream head increases step-wise, the sensors respond depending on the position. Because of seepage through the levee, the upstream head tends to decrease slowly but a constant basin level is attempted by periodic filling. When the pipe tip approaches a transducer, the graph shows a drop in head. This behavior is also observed in Parekh et al. (2016). When the tip passes, the head stabilizes because it shows the (relatively constant) pipe head. The circles are not relevant at this point; these are used in the section "Progression Rates" to derive the tip position. Vertical lines indicate the phases of regressive erosion, progressive erosion, and widening. The transition from regressive to progressive is chosen at the time that the erosion no longer stabilizes. The maximum upstream head is slightly higher.

Note that the head at P9 is not consistent with the other locations. The transducers' spacing is 0.80 m from P3 to P12, so the head difference between those sensors should be similar. The head of P9 is about 0.05–0.10 m too close to P10 during the progressive phase. Possible causes are a poorly compacted zone, preferential flow through coarse sand, or an error in the position of the sensor. In the rest of the analysis, the original values of P9 are used.

The average hydraulic gradient, i, between transducer pairs follows from the head difference and the distance between transducers. In the rest of this paper, gradient indicates the horizontal hydraulic gradient: $i = dh/dx$ (positive for flow toward the exit). Fig. 6 shows three examples, Fig. S3 contains all transducer pairs. Initially, the gradients increase with increasing upstream head. Pipe erosion leads to a decrease in head in the transducer just upstream of the pipe tip and an increase in gradient between the two transducers upstream of the pipe. A clear example is the gradient between P7 and P8 (gradient $i_{7,8}$), which peaks at the moment the pipe reaches P7.

Figs. S4 and S5 show longitudinal head profiles at several points in time, which could be useful for the validation of the gradient in the pipe and upstream of the pipe tip. The pipe gradient is approximately 0.12, and the gradient over the first 0.8 m upstream of the pipe tip varies between 0.31 and 0.41.

Exit Loss

The head loss over the exit hole is estimated as the difference between the downstream water level (0.18 m) and the head at transducer P1. This is an underestimation of the exit loss, because the head at P1 may be slightly higher than the head below the exit, but is expected to be small because there will be little flow from P1 to the exit. The exit loss is approximately 0.1 m during the regressive phase. During the progressive phase, it increases gradually to 0.13 m at the transition to the widening phase and 0.20 m just before the end of the test. This increase may be explained by the

J. Geotech. Geoenviron. Eng., 2021, 147(2): 04020168

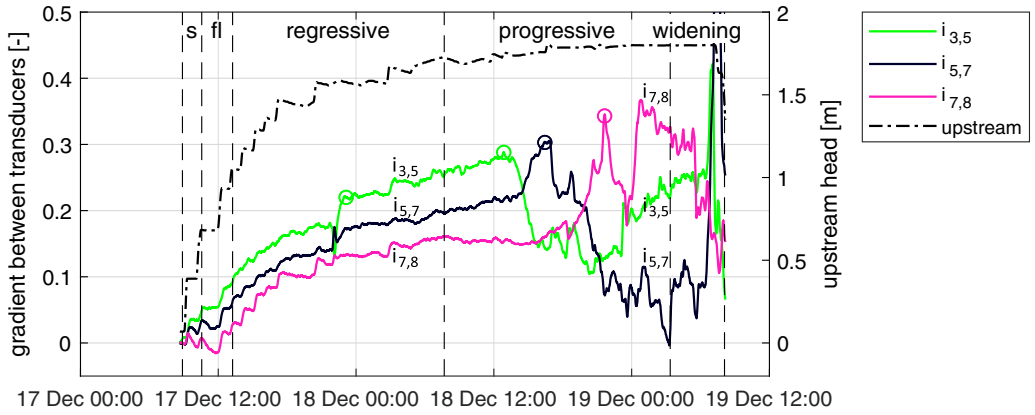

Fig. 6. Average hydraulic gradient between three transducer pairs in the central row. Circles indicate assumed peak in gradient. s = seepage; and fl = fluidization.

increasing sand transport, which leads to more exit resistance (Robbins et al. 2020). As the cover thickness is 0.35 m, the vertical gradient over the exit hole varies between 0.3 and 0.6.

Critical Head

The exit hole fills with fluidized sand at a head difference of 0.5 m. First, sand boil formation is observed at a head difference of 0.85 m. The critical head difference (H_c) at which erosion does not stop anymore is estimated at 1.52 m (1.7 m upstream, 0.18 m downstream head). Correction for 0.10 m exit head loss reduces H_c further to 1.42 m. This observed value is compared to numerical model predictions of MSeep version 18.1 (Sellmeijer 2006), as well as the analytical models of Sellmeijer et al. (2011), Bligh (1910), and Hoffmans and Rijn (2017), using the mean soil properties from Table 1. Bligh's creep factor of 15 for moderate fine sand is corrected for the implicit safety factor in Bligh's design rule (Kanning 2012), which yields a creep factor of 10. The predicted critical head differences are 1.80 m (MSeep), 1.60 m (Sellmeijer et al. 2011), 0.72 m (Bligh 1910), and 1.30 m (Hoffmans and Rijn 2017). All predictions are without 0.10 m exit resistance. Note that larger differences between predicted and observed values do not necessarily indicate that these models perform less well in field situations. Some of these models were derived or calibrated for situations that differ from this test in terms of aquifer geometry and exit type. So the results should be viewed primarily as an indication of how robust the prediction is in different configurations.

Progression Rates

Derivation of Pipe Tip Position

Because a pipe causes a drop in pore pressure, the pipe tip position can be derived from changes in head and gradient in time. This only applies in case the pipe is sufficiently close to the sensor, which was ensured by the guides. The moment that the pipe reaches a transducer can be based on pressure stabilization (Parekh et al. 2016) or peak gradients (Robbins et al. 2017). In the pressure stabilization method, the pipe passes the nth transducer when the head, h_n, stabilizes after a pronounced decrease. In the peak gradient method, the pipe passes the nth transducer when the gradient $i_{n,n+1}$ peaks after a gradual increase and before a pronounced decrease.

The passing times of the pressure stabilization and peak gradient methods are determined visually from Figs. 5 and 6 respectively, and are indicated by circles in those figures. After the passing time, the pressure fluctuates more strongly, which may be caused by temporal clogging or pipe meandering. Fig. 7 shows the development of the pipe tip position by plotting the sensor positions against the passing times (x is distance from the downstream end of the sand bed; Fig. 4). The moment of initiation is plotted with the exit location ($x = 1.3$ m). P1 has no pipe passing because it is located behind the exit. The passing time of the two most downstream transducers, P2 and P3, was more difficult to identify. During the assumed passing of P2 the flow is not stationary yet and therefore a

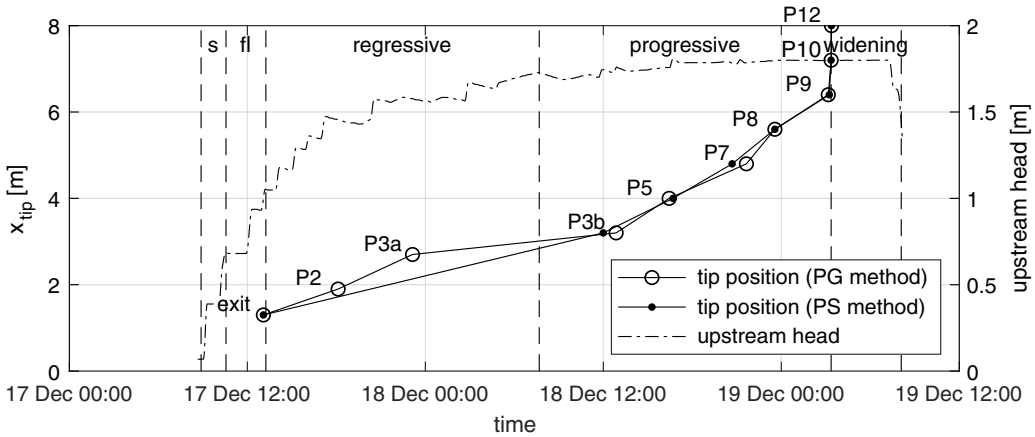

Fig. 7. Development of pipe tip position using peak gradient (PG) and pressure stabilization (PS) methods. s = seepage; and fl = fluidization.

J. Geotech. Geoenviron. Eng., 2021, 147(2): 04020168

pressure stabilization is hardly identifiable. During the assumed passing of P3 the erosion process is very slow (confirmed by erosion volumes), which gives a prolonged increase in gradient instead of a sharp peak. Therefore it is chosen to assign a point P3a at the moment that the pressure starts to increase strongly (December 17, 22:00) in addition to point P3b at the peak before the gradient drops (December 18, 12:00). Since these two transducers mostly reflect the regressive phase, these do not influence the analysis for the progressive phase.

Fig. 7 shows that both methods (peak gradient and pressure stabilization) give very consistent results, and passing times are increasing with x-position as expected. The results are more consistent than the earlier IJkdijk-experiment (Parekh et al. 2016), probably because the pipe is closer to the transducers and there is a single pipe instead of a network. For further analysis, the results of the peak gradient method are used.

Progression rates can be determined from the slope of the lines in Fig. 7. The average progression rate after P3b is passed is approximately 0.1 mm/s, with a maximum of 2 mm/s in the last 1.6 m. Note that the progression rates during the regressive phase are not representative because the time of the transducer passing is relatively uncertain and the rate depends on the head increase interval.

The critical pipe length is the length corresponding to H_c, when the erosion process is just in equilibrium. This results in a slow progression rate, and is the case during the approach of P3: an almost horizontal line between $x_{tip} = 2.7$ m and $x_{tip} = 3.2$ m in Fig. 7. In further analysis, the average is used: $x_{tip} = 2.95$ m. The pipe length, l, is the difference between x_{tip} and x_{exit} (1.3 m), so the observed critical pipe length is $l_c = 2.95 - 1.3 = 1.65$ m. MSeep predicts $l_c = 1.55$ m, which is close to the observed value. Both Sellmeijer's and Bligh's design rules predict no critical pipe length. The observed l_c is smaller than the commonly assumed $1/3L - 1/2L$ (Sellmeijer and Koenders 1991) because of the low ratio of aquifer depth to seepage length (D/L).

Progression Rate as a Function of Local Gradient

Some authors expect that the progression rate is governed by primary erosion and depends on the local hydraulic gradient or pore velocity just upstream of the pipe tip (Kézdi 1979; Robbins et al. 2017). Fig. 8 shows these relationships for the transducers that were passed during the progressive phase (P3–P10). The right axis indicates the pore velocity just upstream of the pipe tip, which equals $u_{p,tip} = k \cdot i_{tip}/n$. The line indicated by $v_{c,avg}$ is the average progression rate during the progressive phase. This value is relatively high because of the high progression rate at the end of the test.

The data seem to confirm a relationship between tip gradient and progression rate for transducers P3–P9, but there are also some outliers. Probably the tip gradients for P8 and P9 in Fig. 8 are overestimated and underestimated, respectively, because of the bias in sensor P9 (noted in the section "Pore Pressure Development"). Furthermore, the peak gradients are expected to increase monotonously with x-position (and thus transducer number) because the seepage path becomes shorter. The deviation of P8 and P9 from this trend supports the hypothesis that these values should be more in line with P3–P7. P10 shows a much higher rate, but this outlier is likely because of the near breach conditions. The overall pattern shows an increase in progression rate with tip gradient, but without sufficient data to fit a reliable relation. Because of the uncertainty, this relationship should be tested in a more controlled laboratory experiment.

Erosion Volumes and Pipe Dimensions

This section aims to estimate the pipe geometry based on the measurements of pipe length and mass of eroded sand (Fig. 9). The measured dry sand mass M (kg) is converted to initial soil volume V_{exp} (m^3) by

$$V_{exp} = \frac{M}{\rho_s(1-n)} \tag{2}$$

The solid line in Fig. 9 shows the measured erosion volume. Initially, the erosion accelerates, 15 h after the start it slows down, and during the progressive phase it accelerates again. Note that, in the regressive phase, the volume increase depends on the applied head increments. Fig. S6 shows the same volume against pipe length.

Two simple models, m1 and m2, are defined for the pipe volume as function of pipe length. Eq. (3) represents a pipe with constant cross-sectional area, A_0. Eq. (4) represents a combination of an ellipsoid when the pipe length, $l \le l_t$, which transitions to a pipe with a constant area, A_0, for $l > l_t$. The coefficient A_d represents the length-width-depth ratio of the ellipsoid

$$V_{m1}(l) = A_0 l \tag{3}$$

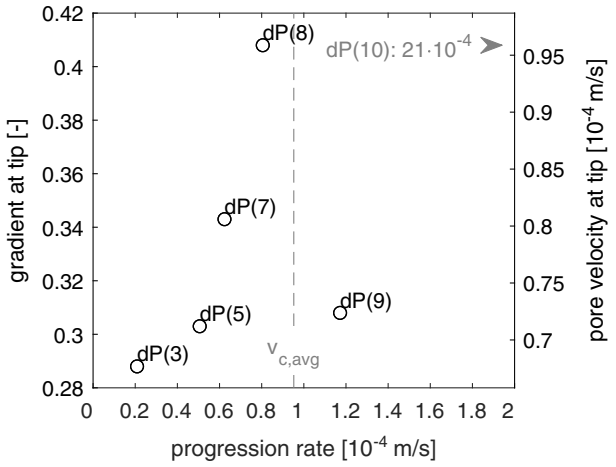

Fig. 8. Progression rate as function of gradient and pore velocity just upstream of the pipe tip, calculated over 0.8 m (transducer spacing).

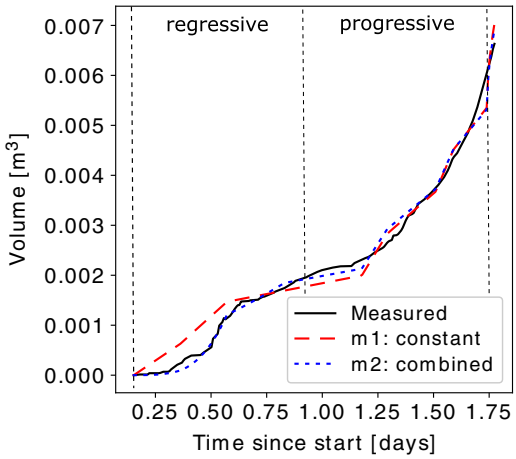

Fig. 9. Measured and modeled erosion volume as function of time.

Table 2. Applied pipe geometry models

Geometry	Best fit coefficients	RMSE (m^3)
Eq. (3): constant	$A_0 = 0.001$ m^2	$2.5 \cdot 10^{-4}$
Eq. (4): combined	$A_0 = 0.001$ m^2, $A_d = 2.7 \cdot 10^{-5}$, $l_t = 1.60$ m	$1.5 \cdot 10^{-4}$

$$V_{m2}(l) = \begin{cases} \frac{16}{3}\pi A_d l^3, & \text{if } l \le l_t \\ \frac{16}{3}\pi A_d l_t^3 + A_0(l - l_t), & \text{if } l > l_t \end{cases} \quad (4)$$

The coefficients in Eqs. (3) and (4) result from minimizing the RMSE between measured $V_{exp}(t)$ and modeled $V_{m1}(t)$ or $V_{m2}(t)$. Table 2 and Fig. 9 show the best fit of each model. The fitted value of $l_t = 1.60$ corresponds to the critical length of 1.65 m which was based on the pressure response. The combined model [Eq. (4)] fits the measurements slightly better than the constant model [Eq. (3)], but especially after the transition to the progressive phase (1.60 m) the difference is negligible. So after an initial increase, the ratio of volume over length or the average cross sectional area is relatively constant.

Discussion

Uncertainties in Measurements

Important results such as progression rates and tip gradients are based on the pore pressure measurements. There are some uncertainties in these data that also affect the results to some extent. First, as discussed in the section "Pore Pressure Development," the head at P9 is probably too high, so gradient $i_{8,9}$ will be too high and $i_{9,10}$ too low. Without this uncertainty, the relation between progression rate and local tip gradient in Fig. 8 is expected to be stronger. Second, the actual pipe head can be lower than the measured pipe head if the pipe passed the sensor at some distance. This does not affect the (average) progression rate, but can be an explanation for the spatial variation in gradients after the pipe passed (Figs. 6 and S3). Third, it should be noted that the calculated gradient is affected by the transducer spacing (0.8 m and thus averaged over this distance) so the actual gradients close to the tip will be larger. Furthermore, the pressure data smoothing (window size) slightly reduces the peak gradients (e.g., in Fig. 8, up to 6%), but it has no effect on the progression rate or the conclusions. Finally, the gradients between the most upstream transducers (9,10,12,14) peak almost instantaneously. The resulting high progression rate (2 mm/s) is considered less reliable, but the true development over this last 1.6 m is unclear. If this part is omitted, the average rate will be 0.06 mm/s instead of 0.1 mm/s. These uncertainties in pressure can be reduced by performing similar (laboratory) experiments with more densely spaced pressure transducers and in which the pipe development can be observed visually.

The pattern of coarse sand strips (Fig. 4) gives rise to the following points of attention. First, if the pipe tip touches a coarse strip with higher permeability, the pore pressure on the upstream side of that strip drops too. This increases the uncertainty in tip position. However, the effect on the progression rate is expected to be small as the error is similar at all transducers P3–P12. Second, it is expected that the pipe tends to grow along the coarse strips. In the area between two consecutive strips, it may grow temporarily sideways, which may reduce the progression rate and increase the pipe volume. Finally, the strips with higher permeability may change the groundwater flow field. Because they are thin (0.05 m compared to an aquifer depth of 1.0 m) and have a limited volume (0.07 m^3 compared to an aquifer volume of 11.4 m^3), they will have no significant influence on the bulk conductivity. This is also reflected by the similarity between bulk conductivity (k_{levee}) and fine sand conductivity (k_{lab}), see Table 1. Hence, there may be some local disturbance of the flow field by the strips, but the effect on piping progression is limited since piping progression is mainly determined by the bulk conductivity of the sand aquifer. It is recommended that this limited influence be confirmed using a detailed three-dimensional (3D) piping erosion model, and to search for an experimental setup or measurement technique that allows sufficiently detailed measurements without disturbance of the sample.

Progression Rates in Other Experiments

Based on a compilation of laboratory tests (Van Beek et al. 2011; Sellmeijer et al. 2011; Vandenboer et al. 2019; Robbins et al. 2017; Yao 2014), Pol et al. (2019) proposed two equations for the average progression rate during the progressive phase ($v_{c,avg}$). The rate is a function of loading (global hydraulic gradient), soil properties (hydraulic conductivity, porosity), and empirical coefficients

$$v_{c,avg} = 4 \cdot 10^{-3} \left(\frac{H}{L}\right)^{1.4} \left(\frac{k}{3.4 \cdot 10^{-4}}\right)^{0.57} \quad (5)$$

$$v_{c,avg} = \frac{3.2kH}{nL} \quad (6)$$

The average rate of 0.1 mm/s that is found in the large scale test of this paper (see the section "Progression Rates") is in good agreement with both empirical formulas. Eqs. (5) and (6) yield 0.19 and 0.14 mm/s respectively, and 0.1 mm/s was observed (see solid dot in Fig. 10). These rates are relatively close to the 0.05–0.06 mm/s obtained in the IJkdijk large scale tests on fine sand (Van Beek et al. 2010; Sellmeijer et al. 2011).

Pipe Dimensions

During the progressive phase, the pipe area, A_0, is approximately 0.001 m^2. Assuming that the pipe is not wider than 0.2 m (width of the middle strip of fine sand), the pipe depth is 5 mm, which is about $30 \cdot d_{50}$. This is larger than values found in laboratory experiments with rigid covers (Hanses 1985; Van Beek et al. 2015; Vandenboer et al. 2018; Allan 2018). Pipe depth in these experiments varies approximately from $2 - 20 \cdot d_{50}$, and the pipe width is $20 - 100 \cdot d_{50}$, which yields an area of $40 - 2{,}000 \cdot d_{50}$ ($7 - 360$ mm^2 for the grain size in this test). In contrast to these lab experiments, IJkdijk tests had a clay cover. At the start of the widening phase of IJkdijk Test 3, the eroded sand mass was 80 kg (Van Beek et al. 2010). Based on $l = 15$ m and $n = 0.398$, this equals an estimated average cross-sectional area of 3,300 mm^2. Note that the IJkdijk test had several active sand boils over the aquifer width of 12 m, whereas our test has only one. Given these differences, the erosion volumes of the two large scale tests are similar. It is not entirely clear whether the larger average cross-sectional area compared to lab experiments is only because of scale or also because of the cohesive blanket. A larger aquifer width and depth results in a higher discharge, so it may be expected that pipes are larger as well. The effect of a cohesive blanket could be caused by the blanket roughness or the deformation of the blanket during the test, which leads to more erosion while the pipe dimensions are not increasing.

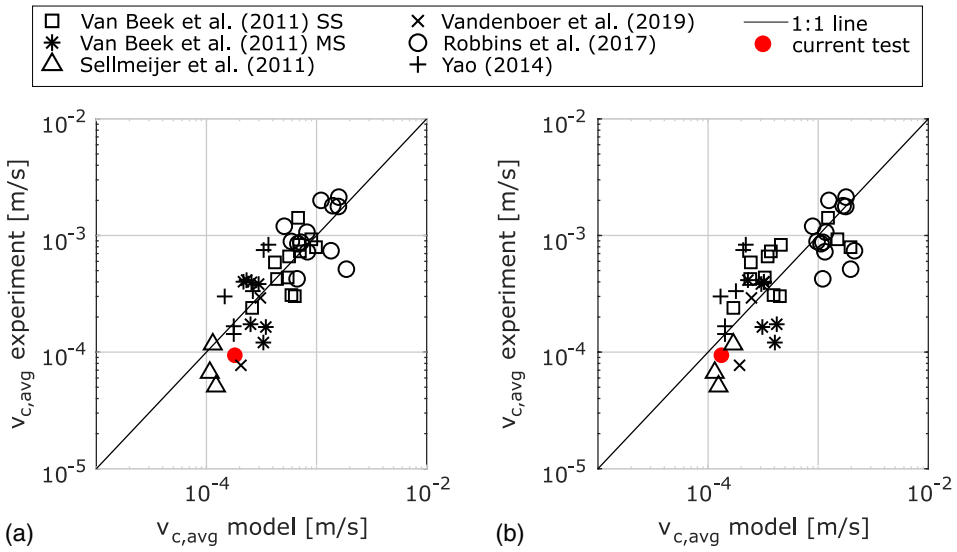

Fig. 10. Average progression rate during the progressive phase compared to other experiments. The progression rate is modeled using (a) Eq. (5); and (b) (Eq. 6). SS = small scale; and MS = medium scale. (Reprinted with permission from Pol et al. 2019.)

Because of the large differences in pipe volumes between laboratory tests with rigid cover and field experiments with cohesive blanket, practitioners should be careful to estimate pipe lengths from observed sand boil volumes in field conditions combined with cross-sectional areas in laboratory tests.

Conclusions

The large scale backward erosion piping experiment described in this paper was designed to study the temporal development of piping in terms of pipe progression rates. The test levee had a 1 m deep sandy aquifer with a seepage length of 7.2 m. Compared to previous experiments, there are two main improvements. First, it had a more realistic, large scale configuration with blanket and hole-type exit. Second, the pipe growth was focused along a row of pore pressure transducers using coarse sand strips, which allows more accurate monitoring of the progression rate.

The performed experiment delivered a useful data set for model validation. First, the experiment confirmed several stages of the piping process described in other research, such as the existence of an equilibrium after initiation (regressive phase) which turns into progressive erosion after a critical head is surpassed. Second, the pipe length development was successfully derived from pore pressure data and shows a consistent trend in the sense that pipe length increases monotonically with time. The average progression rate during the progressive phase (at constant head) was approximately $1 \cdot 10^{-4}$ m/s (8 m/day). This value matches a multivariate regression on previous experiments (Pol et al. 2019). Future research should study the dependence of progression rates on hydraulic loading, scale, and sand properties.

The observed critical head difference, corrected for exit loss, was 1.42 m. The critical pipe length was approximately 1.65 m, which is 23% of the seepage length. It was found that the pipe volume increases linearly with pipe length, after an initial cubic increase. However, the derived average cross-sectional area (approximately $1,000\,\text{mm}^2$) was significantly larger than in small-scale experiments.

An important question for modeling is whether the progression rate is governed by primary erosion or secondary erosion. The results show a relation between tip gradient and progression rate. However, this does not show that the progression rate is governed only by primary erosion, because secondary erosion is also related to the tip gradient. For a better understanding of the dominant drivers, these mechanisms should be studied in more controlled laboratory experiments.

Information on the temporal development can be applied to, for example, levee safety assessments, emergency response planning, and prioritization of monitoring in the most critical levee sections. The relatively slow progression observed in this experiment indicates the importance of the temporal aspects. If similar rates occur in the field, it takes approximately 1 week for a pipe to develop through 50 m seepage length of a levee. In areas with shorter flood duration, this has a significant positive impact on the calculated safety against piping and thus on reinforcement costs.

Current piping models should be extended with temporal development, based on further laboratory experiments that show dependence on hydraulic loading, scale and sand properties. Although the dimensions of this test (mainly the aquifer) are still smaller than in many field situations, the experiment provides a novel data set to validate or benchmark piping models.

Data Availability Statement

All data and code generated or used during the study are available from the corresponding author upon request.

Acknowledgments

This work is part of the Perspectief research programme All-Risk with Project No. P15-21D, which is (partly) financed by NWO Domain Applied and Engineering Sciences. Levee construction was funded by NWO TTW Grant No. 13861 (SAFElevee) and JSPS KAKENHI Grant No. 17H04936. The authors thank Deltares for the provision of equipment and input on the setup, Myron van Damme, Junji Yagisawa, Madelief Doeleman, Mark van der Krogt, Wouter Jan Klerk and all assistants for their support in organizing the experiment. The valuable comments from two anonymous reviewers and the editor greatly improved this paper.

Supplemental Materials

Figs. S1–S6 are available online in the ASCE Library (www.ascelibrary.org).

References

Allan, R. 2018. "Backward erosion piping." Ph.D. thesis, School of Civil and Environmental Engineering, Univ. of New South Wales.

Bligh, W. 1910. "Dams, barrages and weirs on porous foundations." *Eng. News* 64 (26): 708–710.

Bonelli, S., and N. Benahmed. 2010. "Piping flow erosion in water retaining structures: Inferring erosion rates from hole erosion tests and quantifying the failure time." In *Proc., IECS 2010, 8th ICOLD European Club Symp. Dam Safety*. Innsbruck, Austria: Austrian Committee on Large Dams.

Cheng, N.-S. 2004. "Analysis of bedload transport in laminar flows." *Adv. Water Resour.* 27 (9): 937–942. https://doi.org/10.1016/j.advwatres.2004.05.010.

Danka, J., and L. M. Zhang. 2015. "Dike failure mechanisms and breaching parameters." *J. Geotech. Geoenviron. Eng.* 141 (9): 04015039. https://doi.org/10.1061/(ASCE)GT.1943-5606.0001335.

Foster, M., R. Fell, and M. Spannagle. 2000. "The statistics of embankment dam failures and accidents." *Can. Geotech. J.* 37 (5): 1000–1024. https://doi.org/10.1139/t00-030.

Fujisawa, K., A. Murakami, and S.-I. Nishimura. 2010. "Numerical analysis of the erosion and the transport of fine particles within soils leading to the piping phenomenon." *Soils Found.* 50 (4): 471–482. https://doi.org/10.3208/sandf.50.471.

Hanses, U. K. 1985. *Zur Mechanik der Entwicklung von Erosionskanälen in geschichtetem Untergrund unter Stauanlagen*. Berlin, Germany: Universitätsbibliothek der TU Berlin.

Hoffmans, G., and L. Van Rijn. 2017. "Hydraulic approach for predicting piping in dikes." *J. Hydraul. Res.* 56 (2): 268–281. https://doi.org/10.1080/00221686.2017.1315747.

Jongejan, R., and B. Maaskant. 2015. "Quantifying flood risks in the netherlands." *Risk Anal.* 35 (2): 252–264. https://doi.org/10.1111/risa.12285.

Jongman, B., P. J. Ward, and J. C. Aerts. 2012. "Global exposure to river and coastal flooding: Long term trends and changes." *Global Environ. Change* 22 (4): 823–835. https://doi.org/10.1016/j.gloenvcha.2012.07.004.

Jonkman, S. N. 2005. "Global perspectives on loss of human life caused by floods." *Nat. Hazards* 34 (2): 151–175. https://doi.org/10.1007/s11069-004-8891-3.

Kanning, W. 2012. "The weakest link." Ph.D. thesis, Dept. of Hydraulic Engineering, Delft Technical Univ.

Kézdi, A. 1979. Vol. 25 of *Soil physics: Selected topics—Developments in geotechnical engineering*. Amsterdam, Netherlands: Elsevier.

Kreijns, M., R. Gerardts, and M. Rutten. 2018. "Demonstration sites to speed up innovations in delta technology." *J. Cleaner Prod.* 171 (Jan): 144–146. https://doi.org/10.1016/j.jclepro.2016.02.017.

Miesel, D. 1977. "Untersuchungen zum problem der rückschreitenden erosion als ursache des hydraulischen grundbruches in böden mit inhomogener schichtfolge." In Vol. 1 of *Proc., Veröffent-lichungen des Grundbauinstitutes der Technischen Universität Berlin*, 56–71. Berlin: Technischen Universität Berlin.

Miesel, D. 1978. "Rückschreitende erosion unter bindiger deckschicht." In *Proc., Baugrundtagung 1978*, 599–626. Essen, Germany: Deutsche Gesellschaft für Geo-technik.

Morris, M., W. Allsop, F. Buijs, A. Kortenhaus, N. Doorn, and D. Lesniewska. 2008. "Failure modes and mechanisms for flood defence structures." In *Proc., FloodRisk2008*, edited by P. Samuels, S. Huntington, W. Allsop, and J. Harrop, 693–701. London: Taylor & Francis.

Muller-Kirchenbauer, H. 1980. "Zum zeitlichen verlauf der ruckschreitenden erosion in geschichtetem untergrund unter dammen und stauanlagen." In Vol. 43 of *Proc., Talsperrenbau und bauliche Probleme der Pumpspeicherwerke*, 1–25. Hamburg, Germany: Verlag Paul Parey.

Paprotny, D., A. Sebastian, O. Morales-Nápoles, and S. N. Jonkman. 2018. "Trends in flood losses in Europe over the past 150 years." *Nat. Commun.* 9 (1): 1985. https://doi.org/10.1038/s41467-018-04253-1.

Parekh, M. L., W. Kanning, C. Bocovich, M. A. Mooney, and A. R. Koelewijn. 2016. "Backward erosion monitored by spatial-temporal pore pressure changes during field experiments." *J. Geotech. Geoenviron. Eng.* 142 (10): 04016050. https://doi.org/10.1061/(ASCE)GT.1943-5606.0001528.

Pol, J. C., W. Kanning, and S. N. Jonkman. 2020. "FPH piping experiment December 2018." Accessed May 13, 2020. https://data.4tu.nl/articles/Flood_Proof_Holland_FPH_piping_experiment_December_2018/12692231.

Pol, J. C., V. M. Van Beek, W. Kanning, and S. N. Jonkman. 2019. "Progression rate of backward erosion piping in laboratory experiments and reliability analysis." In *Proc., 7th Int. Symp. on Geotechnical Safety and Risk (ISGSR)*, edited by J. Ching, D. Li, and J. Zhang, 764–769. Singapore: Research Publishing.

Robbins, B. A., I. J. Stephens, V. M. Van Beek, A. R. Koelewijn, and A. Bezuijen. 2020. "Field measurements of sand boil hydraulics." *Géotechnique* 70 (2): 153–160. https://doi.org/10.1680/jgeot.18.P.151.

Robbins, B. A., V. M. Van Beek, J. F. Lopez-Soto, A. M. Montalvo-Bartolomei, and J. Murphy. 2017. "A novel laboratory test for backward erosion piping." *Int. J. Phys. Modell. Geotech.* 18 (5): 266–279. https://doi.org/10.1680/jphmg.17.00016.

Rotunno, A. F., C. Callari, and F. Froiio. 2019. "A finite element method for localized erosion in porous media with applications to backward piping in levees." *Int. J. Numer. Anal. Methods Geomech.* 43 (1): 293–316. https://doi.org/10.1002/nag.2864.

Schmertmann, J. 2000. "No-filter factor of safety against piping through sands." In *Proc., Judgment and Innovation*, edited by F. Silva and E. Kavazanjian, 65–105. Reston, VA: ASCE.

Schweckendiek, T., A. Vrouwenvelder, and E. Calle. 2014. "Updating piping reliability with field performance observations." *Struct. Saf.* 47 (Mar): 13–23. https://doi.org/10.1016/j.strusafe.2013.10.002.

Sellmeijer, H., J. L. de la Cruz, V. M. van Beek, and H. Knoeff. 2011. "Fine-tuning of the backward erosion piping model through small-scale, medium-scale and IJkdijk experiments." *Eur. J. Environ. Civ. Eng.* 15 (8): 1139–1154. https://doi.org/10.1080/19648189.2011.9714845.

Sellmeijer, J. B. 1988. "On the mechanism of piping under impervious structures." Ph.D. thesis, Dept. of Civil Engineering and Geosciences, Delft Univ. of Technology.

Sellmeijer, J. B. 2006. "Numerical computation of seepage erosion below dams (piping)." In *Proc., 3rd Int. Conf. on Scour and Erosion (ICSE-3)*, edited by H. Verheij and G. Hoffmans, 596–601. Gouda, Netherlands: CURNET.

Sellmeijer, J. B., and M. A. Koenders. 1991. "A mathematical model for piping." *Appl. Math. Modell.* 15 (11): 646–651. https://doi.org/10.1016/S0307-904X(09)81011-1.

Shen, J. 1981. *Discharge characteristics of triangular-notch thin-plate weirs*. Washington, DC: USGS.

Tóth, S., and L. Nagy. 2006. "Dyke failures in Hungary of the past 220 years." In *Proc., Transboundary Floods: Reducing Risks Through Flood Management*, edited by J. Marsalek, G. Stancalie, and G. Balint, 247–258. Dordrecht, Netherlands: Springer.

Van Beek, V., H. De Bruijn, J. Knoeff, A. Bezuijen, and U. Förster. 2010. "Levee failure due to piping: A full-scale experiment." In *Proc., 5th Int. Conf. on Scour and Erosion (ICSE-5)*, 283–292. Reston, VA: ASCE.

Van Beek, V., H. Van Essen, K. Vandenboer, and A. Bezuijen. 2015. "Developments in modelling of backward erosion piping." *Géotechnique* 65 (9): 740–754. https://doi.org/10.1680/geot.14.P.119.

Van Beek, V. M. 2015. "Backward erosion piping: Initiation and progression." Ph.D. thesis, Dept. of Civil Engineering and Geosciences, Delft Univ. of Technology.

Van Beek, V. M., H. Knoeff, and H. Sellmeijer. 2011. "Observations on the process of backward erosion piping in small-, medium- and full-scale experiments." *Eur. J. Environ. Civ. Eng.* 15 (8): 1115–1137. https://doi.org/10.1080/19648189.2011.9714844.

Vandenboer, K. 2019. "A study on the mechanisms of backward erosion piping." Ph.D. thesis, Dept. of Civil Engineering, Ghent Univ.

Vandenboer, K., F. Celette, and A. Bezuijen. 2019. "The effect of sudden critical and supercritical hydraulic loads on backward erosion piping: Small-scale experiments." *Acta Geotech.* 14 (3): 783–794. https://doi.org/10.1007/s11440-018-0756-0.

Vandenboer, K., V. M. van Beek, and A. Bezuijen. 2018. "Analysis of the pipe depth development in small-scale backward erosion piping experiments." *Acta Geotech.* 14 (2): 477–486. https://doi.org/10.1007/s11440-018-0667-0.

Van Esch, J., J. Sellmeijer, and D. Stolle. 2013. "Modeling transient groundwater flow and piping under dikes and dams." In Vol. 9 of *Proc., 3rd Int. Symp. on Computational Geomechanics (ComGeo III)*, edited by S. Pietruszczak and G. Pande. London: Taylor & Francis.

Wang, D. Y., X. D. Fu, Y. X. Jie, W. J. Dong, and D. Hu. 2014. "Simulation of pipe progression in a levee foundation with coupled seepage and pipe flow domains." *Soils Found.* 54 (5): 974–984. https://doi.org/10.1016/j.sandf.2014.09.003.

Xiao, Y., H. Cao, and G. Luo. 2019. "Experimental investigation of the backward erosion mechanism near the pipe tip." *Acta Geotech.* 14 (3): 767–781. https://doi.org/10.1007/s11440-019-00779-w.

Yagisawa, J., M. van Damme, J. C. Pol, and J. D. Bricker. 2019. "Verification of a predictive formula for critical shear stress with large scale levee erosion experiment." In *Proc., 11th ICOLD European Club Symp*. Athens, Greece: Greek Committee on Large Dams.

Yao, Q. 2014. "Multi-size experiments and numerical simulation for backward erosion piping in dike foundations." Ph.D. thesis, Dept. of Geotechnical Engineering, China Institute of Water Resources and Hydropower Research.